Received: 2 October 2021 | Revised: 11 January 2022 | Accepted: 27 January 2022

DOI: 10.1111/gbi.12488

gebiology WILEY

ORIGINAL ARTICLE

Widespread mineralization of soft-bodied insects in Cretaceous amber

Hui Jiang[1,2,3] | Frank Tomaschek[4] | A. Drew Muscente[5] | Changtai Niu[1,6] | Thet Tin Nyunt[7] | Yan Fang[1] | Ute Schmidt[8] | Jun Chen[9] | Mara Lönartz[4,10] | Bastian Mähler[3] | Torsten Wappler[3,11] | Edmund A. Jarzembowski[1] | Jacek Szwedo[12] | Haichun Zhang[1] | Jes Rust[3] | Bo Wang[1]

[1]State Key Laboratory of Palaeobiology and Stratigraphy, Nanjing Institute of Geology and Palaeontology and Center for Excellence in Life and Paleoenvironment, Chinese Academy of Sciences, Nanjing, China

[2]University of the Chinese Academy of Sciences, Beijing, China

[3]Section Palaeontology, Institute of Geosciences, Rheinische Friedrich-Wilhelms-Universität Bonn, Bonn, Germany

[4]Section Geochemistry/Petrology, Institute of Geosciences, Rheinische Friedrich-Wilhelms-Universität Bonn, Bonn, Germany

[5]Department of Geology, Cornell College, Iowa, USA

[6]University of Science and Technology of China, Hefei, China

[7]Department of Geological Survey and Mineral Exploration, Myanmar Gems Museum, Ministry of Natural Resources and Environmental Conservation, Nay Pyi Taw, Myanmar

[8]WITec GmbH, Ulm, Germany

[9]Institute of Geology and Paleontology, Linyi University, Linyi, China

[10]Institute of Energy and Climate Research (IEK-6): Nuclear Waste Management and Reactor Safety, Forschungszentrum Jülich GmbH, Jülich, Germany

[11]Natural History Department, Hessisches Landesmuseum Darmstadt, Darmstadt, Germany

[12]Laboratory of Evolutionary Entomology and Museum of Amber Inclusions, Department of Invertebrate Zoology and Parasitology, University of Gdańsk, Gdańsk, Poland

Correspondence
Hui Jiang and Bo Wang, State Key Laboratory of Palaeobiology and Stratigraphy, Nanjing Institute of Geology and Palaeontology and Center for Excellence in Life and Paleoenvironment, Chinese Academy of Sciences, Nanjing 210008, China.
Emails: huijiang2353@163.com (H. J.); bowang@nigpas.ac.cn (B. W.)

Funding information
the Strategic Priority Research Program of the Chinese Academy of Sciences; the Second Tibetan Plateau Scientific Expedition and Research; National Natural Science Foundation of China; Deutsche Forschungsgemeinschaft

Abstract

Fossilized tree resin, or amber, commonly contains fossils of animals, plants and microorganisms. These inclusions have generally been interpreted as hollow moulds or mummified remains coated or filled with carbonaceous material. Here, we provide the first report of calcified and silicified insects in amber from the mid-Cretaceous Kachin (Burmese) amber. Data from light microscopy, scanning electron microscopy (SEM), energy-dispersive and wavelength-dispersive X-ray spectroscopy (EDX and WDX), X-ray micro-computed tomography (Micro-CT) and Raman spectroscopy show that these Kachin fossils owe their preservation to multiple diagenetic mineralization processes. The labile tissues (e.g. eyes, wings and trachea) mainly consist of calcite, chalcedony and quartz with minor amounts of carbonaceous material, pyrite, iron oxide and phyllosilicate minerals. Calcite, quartz and chalcedony also occur in cracks as void-filling cements, indicating that the minerals formed from chemical species that entered the fossil inclusions through cracks in the resin. The results demonstrate that resin and amber are not always closed systems. Fluids (e.g. sediment pore water, diagenetic fluid and ground water) at different burial stages have chances to interact

with amber throughout its geological history and affect the preservational quality and morphological fidelity of its fossil inclusions.

1 | INTRODUCTION

Amber originates from the hardening of resin produced by trees (Langenheim, 2003; McCoy et al., 2018; McCoy, Soriano, Pegoraro, et al., 2018; Sadowski et al., 2021; Seyfullah et al., 2018). If organisms become trapped in the viscous resin before it hardens, they are sometimes preserved as fossil inclusions within the amber. The fossils themselves often represent remains of labile tissues, such as cellular details and cuticles (e.g. Grimaldi et al., 1994; Hartl et al., 2015; Henwood, 1992a, 1992b; Koller et al., 2005; Poinar, 1992; Poinar & Hess, 1982; Rust et al., 2010; Sadowski et al., 2017), making them 'exceptionally preserved' fossils (Briggs, 2003; Muscente et al., 2017). Fossil inclusions in amber receive a great deal of attention in the study of paleoecosystems and evolutionary history (e.g. Briggs, 2018; Ross, 2021; Sadowski et al., 2021) and represent a critical window to the evolution of terrestrial environments across the Mesozoic–Cenozoic transition (e.g. Labandeira, 2014; Martínez-Delclòs et al., 2004; Penney, 2010; Sadowski et al., 2021).

'Exceptionally preserved' fossils in amber may owe their high quality and preservational fidelity to the biocidal properties of resin as well as its role as a 'conservation trap' (Briggs, 2003). Resin protects its inclusions from the physical and biological processes that ordinarily destroy non-biomineralized tissues in terrestrial environments. The amber inclusions are commonly interpreted as mummified remains or hollow moulds, which are sometimes coated or filled with carbonaceous material (e.g. Grimaldi et al., 1994; Henwood, 1992a; Labandeira, 2014; Martínez-Delclòs et al., 2004; McCoy, Soriano, & Gabbott, 2018; McCoy, Soriano, Pegoraro, et al., 2018; Poinar, 1992; Poinar & Hess, 1982; Sadowski et al., 2021; Stankiewicz et al., 1998). These mummified inclusions and moulds could remain organisms' cells, tissues and organs in high fidelity, and these organic matters undergo molecular polymerization ('carbonization' or 'kerogenization') and survive as carbonaceous material on the body cavities and walls of the moulds. This paradigm, however, may not apply to all amber. A number of reports have described amber containing mineralized inclusions, including pyritized insects in Eocene Baltic amber (Baroni-Urbani & Graeser, 1987; Kowalewska & Szwedo, 2009), pyritized pseudoinclusions in Lower Cretaceous Spanish amber (e.g. Lozano et al., 2020; Martín-González et al., 2009), possibly pyritized liverwort in mid-Cretaceous Kachin amber (Sadowski et al., 2021; Seyfullah and Schmidt, 2015) and a phosphatic lizard bone in Miocene Dominican amber, which evidently, underwent a transformation from bioapatite to fluorapatite (Barthel et al., 2020). Such mineralized inclusions in amber have not received much attention, as they are typically considered to be 'very rare' (Briggs, 2003). The mineralized fossils may alternatively reflect a gap in knowledge about the taphonomy of amber. In either case, such fossils may provide insights to the taphonomic processes that affect the preservation of soft-tissues in amber.

In this study, we examine a variety of fossils from mid-Cretaceous Kachin amber. The fossils were collected from an amber mine near Noije Bum Village, Tanai Town, in northern Myanmar. This amber biota is currently one of the most biodiverse fossil sites in the fossil record (Ross, 2021), which includes abundant invertebrates, vertebrates and plants, but the taphonomy of the fossils in this biota has received little attention. Here, we first report the calcification and silicification of insects in amber and examine the roles of diagenetic processes in the preservation of amber and its inclusions.

2 | MATERIALS AND METHODS

2.1 | Material

Amber pieces (MGM2016–011, MGM2016–012, MGM2016–013, MGM2016–014, MGM2016–015, MGM2016–016, MGM2016–017 and MGM2016–018) are permanently deposited in the Myanma Gems Museum, Nay Pyi Taw, Myanmar. They were collected from the Angbamo site, Tanai Township, Myitkyina District, Kachin Province of Myanmar from 2013 to 2016, before the Myanmar army closed the Kachin amber mines in November 2017. The fossils were acquired in full compliance with the laws of Myanmar. All authors declare that the amber reported in this study is not involved in armed conflict and ethnic strife in Myanmar.

2.2 | Geological setting

The Kachin amber occurs in the fine clastic facies of fine or very fine-grained sandstone (grains usually 0.1 mm or less), with beds of finer clastics (silt, shale), interbeds of grey micritic limestone a few centimetres thick and coal laminations usually about 1–2 mm thick (Cruickshank & Ko, 2003). According to U–Pb dating of zircons from the volcanoclastic matrix, the amber has a maximum age of 98.8 ± 0.6 million years (Shi et al., 2012), and the biostratigraphy of an ammonite trapped in the amber corroborates a mid-Cretaceous age (Yu et al., 2019). Given the faunal elements and facies of the surrounding rock, the fossils were likely preserved in a nearshore marine environment (Cruickshank & Ko, 2003).

2.3 | Fossil preparation

The amber pieces were broken open to expose the inclusions along their surfaces, and a number of pieces (n = 2) were prepared as

petrographic thin sections for study with transmitted light microscopy. The termite specimen (MGM2016–012) was cross sectioned into two pieces across the sagittal section of the body. One piece was prepared as a polished thick section for direct observation with reflected light microscopy, and the other was prepared as a petrographic thin section for transmitted light microscopy. The click beetle specimen (MGM2016–015) was sectioned along the transverse plane across its thorax and abdomen, and a petrographic thin section was prepared from the most anterior part of the insect body.

2.4 | Light microscopy

Reflected light micrographs were acquired using a Zeiss AXIO ZoomV16 stereo microscope system. To ensure that images of the 3-dimensional (3D) structures of the fossils contained a high depth of field, each image was produced using a procedure, wherein, images were taken at approximately 40–60 individual focal planes were digitally stacked and combined together with the Helicon Focus 7 software. Fluorescence images were obtained under the illumination of a 395 nm wavelength UV lamp. Transmitted light microscopic analyses with parallel and cross polarized light were carried out with a Zeiss Axio Imager. A1 microscope, equipped with a Panasonic Lumix camera.

2.5 | Electron microscopy and chemical analyses

Backscattered electron scanning electron microscopy (BSE) images of five fossil samples (MGM2016–011, MGM2016–012, MGM2016–014, MGM2016–016 and MGM2016–018) were obtained using two SEM systems at the State Key Laboratory of Palaeobiology and Stratigraphy, NIGPAS: a LEO 1530VP SEM and a TESCAN MAIA 3 GMU SEM with field emission electron source and Oxford Aztec 170 mm^2 spectroscope for energy-dispersive X-ray spectroscopy. The BSE images were acquired at acceleration voltages of 5–20 keV and working distance between 5.5 and 10.5 mm; they were acquired in low and high vacuum modes in the LEO 1530VP and TESCAN MAIA systems respectively.

Additional BSE and panchromatic cathodoluminescence (CL) images were obtained using a Jeol 8200 Superprobe electron microprobe at the Institute of Geosciences, University of Bonn. These data were collected from carbon-coated, polished sections of two samples (MGM2016–012 and MGM2016–015) using 15 keV accelerating voltage and 15 nA beam current. Wavelength-dispersive X-ray (WDX) intensity maps were acquired for several elements, including C, S, Ca and Mg, using a focussed beam, step size of 2 μm and 120 ms dwell time.

2.6 | Raman spectroscopy

Raman spectra were obtained using a WITec alpha300 R confocal Raman imaging microscope at the Wissenschaftliche Instrumente und Technologie GmbH, and a Horiba Scientific LabRAM HR800 confocal Raman spectrometer at the Institute of Geosciences, University of Bonn. Excitation was provided by a monochromatic laser beam with a wavelength of 532, 633 and 784 nm respectively.

2.7 | X-ray microcomputed tomography (Micro-CT)

Micro-CT scanned for four specimens (MGM2016–011, MGM2016–012, MGM2016–013 and MGM2016–016) was obtained using a 3D X-ray microscope (3D–XRM), Zeiss Xradia 520 Versa at the State Key Laboratory of Paleobiology and Stratigraphy, NIGPAS. Images were generated using CCD-based 4x (MGM2016–011) and 0.4x (MGM2016–012, MGM2016–013 and MGM2016–016) objectives at an X-ray voltage of 50 kV (power 4W) or 60 kV (power 5W, MGM2016–013), with isotropic voxel sizes of 4.59, 14.09, 9.09 and 15.79 μm respectively. Samples MGM2016–012 and MGM2016–015 were scanned using a phoenix v|tome|x s micro-CT at the Institute of Geosciences, University of Bonn. Images of MGM2016–012 and MGM2016–015 were generated by a CCD-based 20x objective and at an X-ray voltage of 80 kV (120 mA) with the voxel size 7.59 and 5.06 μm respectively. To improve the signal-to-noise ratio, data for each specimen were collected over 360° and taken in 1492–2501 projections. The exposure time for each projection was between 1 and 5 s. Volume data processing was performed using the software Avizo 8.1 (FEI Visualization Sciences Group) and VGStudio Max (version 3.0, Volume Graphics).

3 | RESULTS

The eight randomly investigated amber pieces contain insect inclusions representing the following five orders: Orthoptera, Blattodea, Neuroptera, Hemiptera and Coleoptera. These specimens represent some of the common taxonomic groups in the Kachin amber (Grimaldi et al., 2002; Ross, 2021). In backscattered electron (BSE) images, which have high compositional contrast and low topographic contrast (Muscente & Xiao, 2015), the fossils appear brighter than the surrounding amber (Figures 1h,k and 2d), indicating that they consist of a material with greater average atomic number (Z) than the fossilized resin. Because these materials have higher rates of X-ray attenuation than the surrounding amber, the acquisition of detailed images and three-dimensional reconstructions of these fossils with micro-CT is fairly straightforward (Figures 1b, 2c and 4b,i) relative to such work on inclusions consisting of carbonaceous material. Evidently, the fossils are not hollow moulds, but rather, solid inclusions made of high-Z materials. Data from transmitted–light microscopy, EDX, WDX and Raman spectroscopy show that the fossils consist of calcite ($CaCO_3$) and two varieties of silica ($SiO_2{}^*nH_2O$): microcrystalline (chalcedonic) quartz and macrocrystalline quartz. In the inclusions, the minerals occupy the positions of numerous tissues and substrates, occurring as replacement minerals in the organic structures as well as void-filling cements in the cavities within

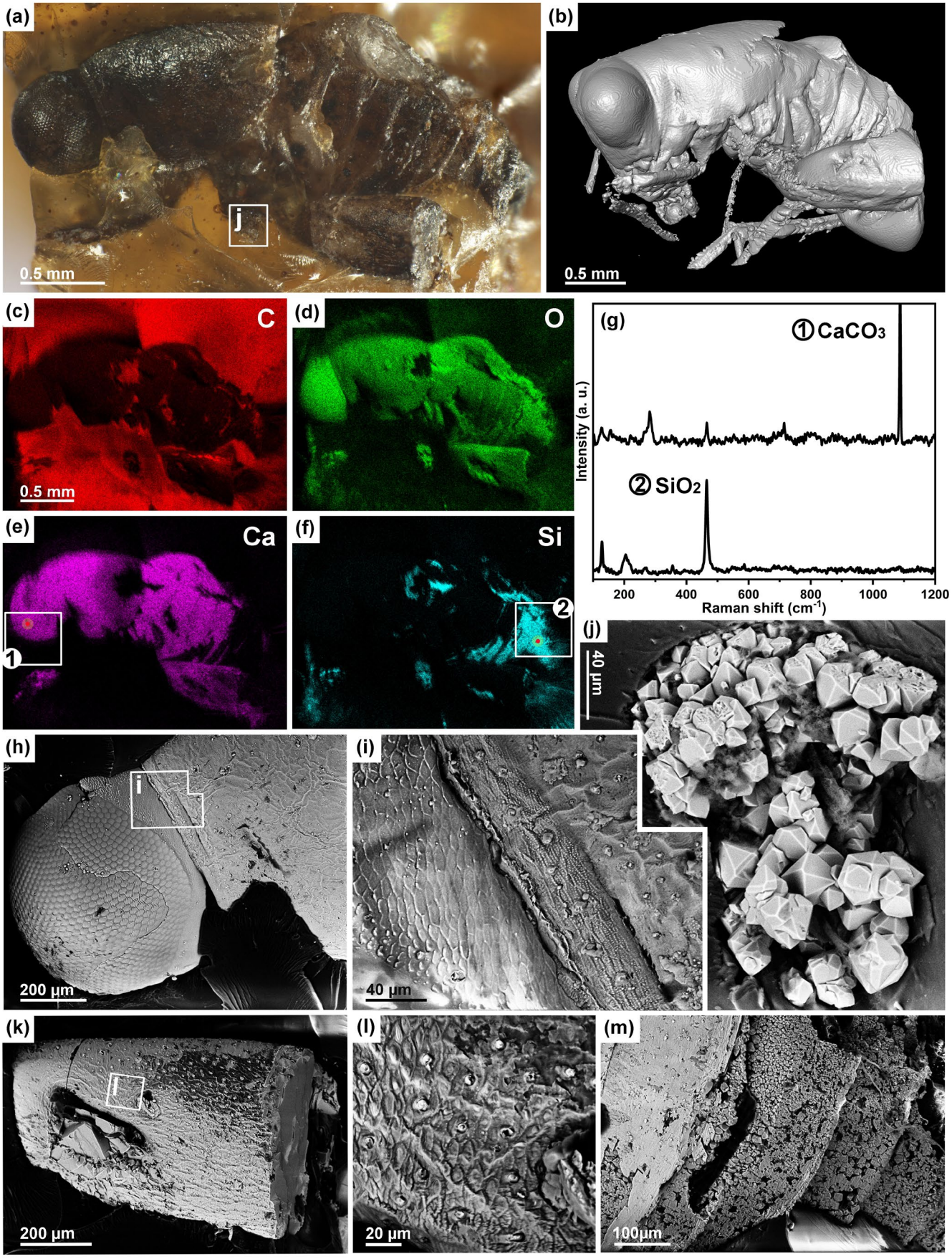
(a)
j
0.5 mm
(b)
0.5 mm
(c)
C
0.5 mm
(d)
O
(e)
Ca
1
(f)
Si
2
(g)
①CaCO3
②SiO2
Intensity (a. u.)
200
400
600
800
1000
1200
Raman shift (cm-1)
(j)
40 μm
(h)
i
200 μm
(i)
40 μm
(k)
l
200 μm
(l)
20 μm
(m)
100μm

FIGURE 1 Calcified and silicified long-horn grasshopper (Orthoptera: Elcanoidea) nymph (MGM2016–011). (a) Reflected light micrograph of opened inclusion in left lateral view. (b) Left lateral view of microtomographic reconstruction. (c–f) EDX elemental maps for C (c), O (d), Ca (e) and Si (f) of the left lateral view. (g) Raman spectra of calcium carbonate and quartz from regions indicated in (e) and (f). (h–m) Backscattered electron microscopy (BSE) images. (h) The compound eye and part of pronotum. (i) Magnified view of the box in (h), showing the connection between the posterior part of the head and the anterior part of the pronotum. (j) Magnified view of the box in (a), showing quartz grains outside the body. (k) Lateral view of left femur. (l) Magnified view of the box in (k), showing the cuticle of left femur. (m) The fourth to seven segments of the abdomen, showing calcified cuticle and quartz crystals

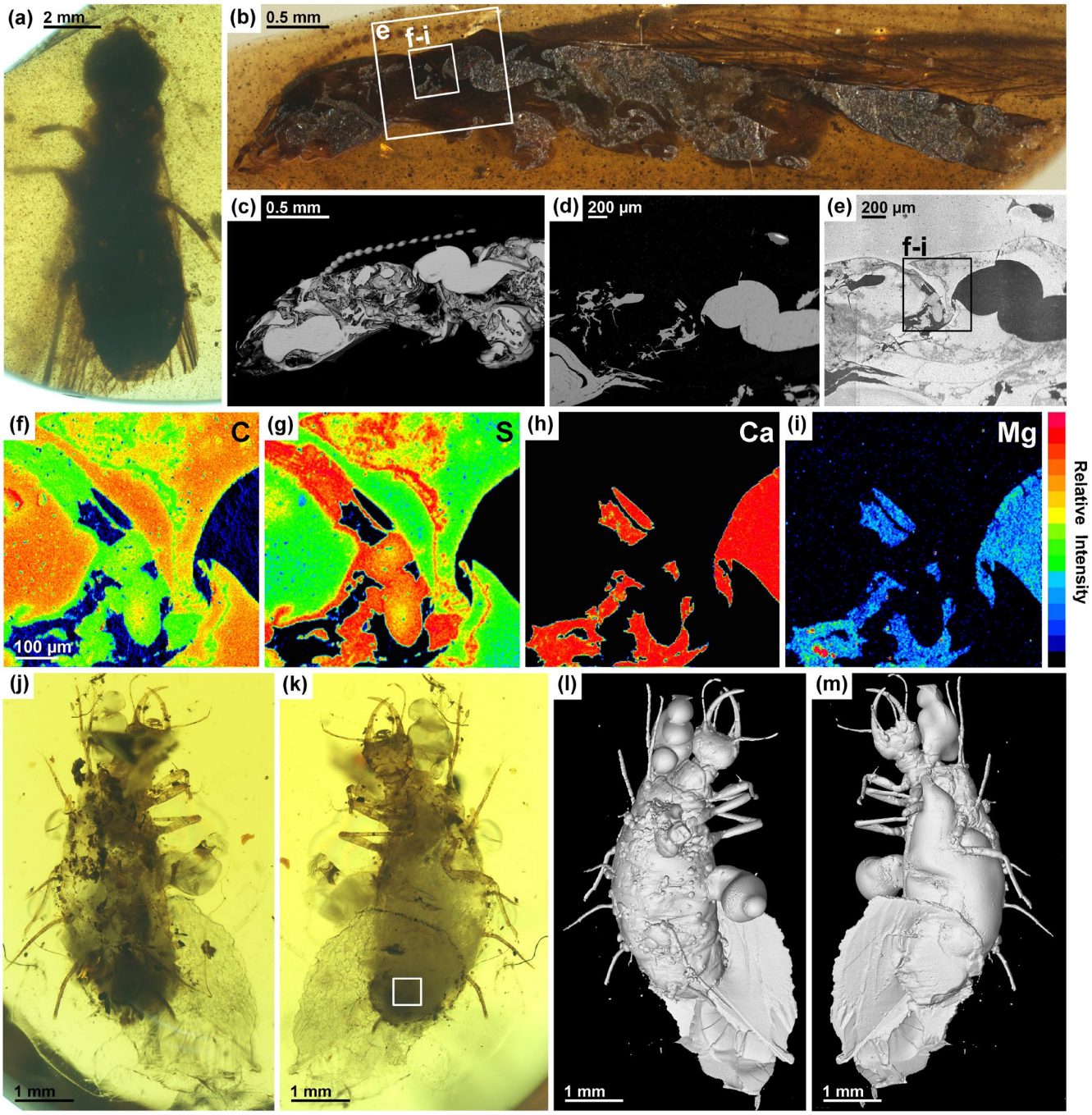

FIGURE 2 Calcified fossils. (a–g) Termite (Blattaria: Stolotermitidae) (MGM2016–012). (a–b) Reflected light micrographs of dorsal view of intact specimen (a) and sagittal section of right side of body (b). (c) Sagittal section of right side of body forequarters in a microtomographic reconstruction. (d) BSE image of box in a, showing mineralized (high-Z) areas. (e) CL image of box in (b), showing part of the head connected with the thorax. (f–i) Wavelength-dispersive X-ray intensity (WDX) maps of the boxes in (b) and (e) for C (f), S (g), Ca (h) and Mg (i). (j–m) Lacewing larva (Order Neuroptera) of the superfamily Chrysopoidea (MGM2016–013). (j–k) Reflected light micrographs of dorsal (j) and ventral (k) views. (l–m) Microtomographic reconstruction in dorsal (l) and ventral (m) views. Raman analytical points indicated on the box in (k)

the insects' bodies. The minerals also occur within cracks that cross-cut the fossils and amber matrix.

The long-horn grasshopper nymph (Orthoptera: Elcanoidea) specimen consists of both calcite and quartz (Figure 1) and displays vitreous lustre with darkbrown organic matter residues. Elemental maps acquired with EDX show that, in general, the fossil contains lower concentrations of C than the amber matrix (Figure 1c), with the exception of areas of the body that are covered or infilled by amber. In addition, the data show that the fossil contains variable concentrations of O, Ca and Si (Figure 1d–f), including areas of high concentrations of O and Si (and low concentrations of Ca and C) as well as Ca-rich areas (with low concentrations of Si and C). Raman spectroscopy confirms that these Ca- and Si-rich areas consist of calcite and quartz respectively (Figure 1g). BSE images and EDX elemental maps show that the well-preserved body structures are calcified (Figure 1h,i,k–m), like the compound eye of the specimen, which retains an intact and regular hexagonal array of ommatidia facets (Figure 1h). Other calcified structures include the head's polygonal pattern of the posterior cuticle (Figure 1i); the thoracic verrucous anterior micro-relief plus tactile sensillae and pore sensillae (Figure 1i); and the cuticle of femur with tactile sensilla, pores and regular polygon patterns (Figure 1k,l). The last five segments of the abdomen mainly consist of quartz (Figure 1m), which is also present inside the femur and body cavities and outside the body (Figure 1j). The quartz occupies the space of the gross morphology of the abdominal segments but lacks their fine ultrastructural details (Figure 1m); the silicified body parts are not preserved with the same degree of morphological fidelity as the calcified tissues and substrates. The size of the quartz grains varies greatly from 1 μm to more than 100 μm. Some of the quartz crystals have euhedral terminations (Figure 1m), suggesting that they grew into open spaces. Other crystals nucleated and grew on the calcified cuticle.

Images of the termite (Blattodea: Stolotermitidae) fossil (Figure 2a,b), acquired with transmitted polarized and cross polarized light, show that the body cavity is mainly mineralized with calcite, which exhibits twinning planes and a maximum interference colour of pearl grey (Figure S1b–d). The micro-CT reconstruction of this fossil documents the presence of a membranous connection between head and thorax (Figure 2c); the fragmented appearance of the connection appears to reflect the incomplete replacement of organic matter with calcite. Cathodoluminescence imaging (CL) reveals three distinct domains in the area connecting the head to the thorax—the amber matrix, the insect's carbonaceous material residue and diagenetic calcite—which differ in their greyscale appearance in BSE and CL images (Figure 2d,e). Elemental maps acquired with WDX also provide evidence of three types of materials (Figure 2f–i). Whereas the calcite contains high concentrations of Ca and Mg (and low concentrations of C and S), the amber and insect carbonaceous residue both contain high concentrations of C and S (and low concentrations of Ca and Mg). Nonetheless, the insect residue contains relatively more S (and less C) than the amber, and vice versa. Calcite crystals occur as replacement minerals occupying the place of organic tissue and (Figure 2f–h) and as void-filling cements in body cavities.

Another specimen is a green lacewing larva (Neuroptera: Chrysopoidea). The micro-CT reconstruction of this fossil highlights the morphology of the mineralized larva and surrounding minerals (Figure 2j–m). In the area around its thorax and abdomen, irregular rounded protrusions are present, which may be bubbles around the insect. The amber matrix around the lower part of the abdomen has a sheet-like structure, showing that minerals may have precipitated along cracks in the amber in contact with the insect. The sample is not cracked, but our Raman spectroscopy identified crystals exposed at the edge of the amber specimen as calcite (analytical area indicated on Figure 2k).

The other five specimens largely consist of quartz and chalcedony. The amber matrix surrounding the cicada (Hemiptera: Cicadoidea) is cloudy and contains mineralized cracks with glassy lustre (Figure 3a). Electron images, EDX elemental maps of C, O and Si (Figure 3c–f) and Raman spectroscopy (Figure 3g) suggest that the cicada wing consists of quartz crystal aggregates. The veins and membrane of the forewing and hindwing replaced by quartz are visible in BSE-SEM images (Figure 3h–i). EDX elemental maps show that a crack within the amber around the cicada body is filled with quartz (Figure 3k–n), which appears bright and reflective under UV light (Figure 3j).

The click beetle (Coleoptera: Elateridae) consists of agate. The specimen was cut along a transverse direction across thorax and abdomen (Figure 4a–c). The most anterior part of the insect was prepared into a thin section (Figure 4e–g). The beetle's body cavity is filled with agate, consisting of milky white to transparent grey layered chalcedony, and a core of well-developed, clear quartz crystals (Figure 4d). The wall surrounding the body cavity is comprised of carbonaceous material. Observations from transmitted, cross polarized light microscopy support the interpretation of the fibrous microcrystalline silica as length-fast chalcedony (Figure 4f–g), and Raman spectroscopy affirms that the isopachous cements consist of microcrystalline quartz (chalcedony) without a moganite component (Figure S2a,e). The wall and cavity of the hind leg tibia also consist of microcrystalline quartz, as indicated by BSE images where they appear as a high-Z material. Mineralization both replaced the cuticle and supplemented the exoskeletal structure of the tibia (Figure S2b,c).

Drywood termite (Blattodea: Kalotermitidae) specimen (Figure 4h–i) is similar to the click beetle that their internal body cavities resemble a geode with microcrystals lining the walls and macrocrystals occupying the centre of the cavities (Figure 4j,k). Electron imaging EDX elemental mapping and Raman spectroscopy demonstrate that the interior of the termite body consists of micro- and macrocrystalline quartz (Figure 4k, Figure S2e–h). The areas consisting of microcrystalline quartz retain finer details of the inner body than those with macrocrystalline quartz. Fine details in this specimen include fibre structure, mesh-like structure and tracheae (Figure 4l–n); the spiral chitin, which stabilizes the tracheal walls, now consists of microcrystals (Figure 4m).

The silicified insects contain carbonaceous material and are encrusted by a number of additional minerals. Raman analysis and

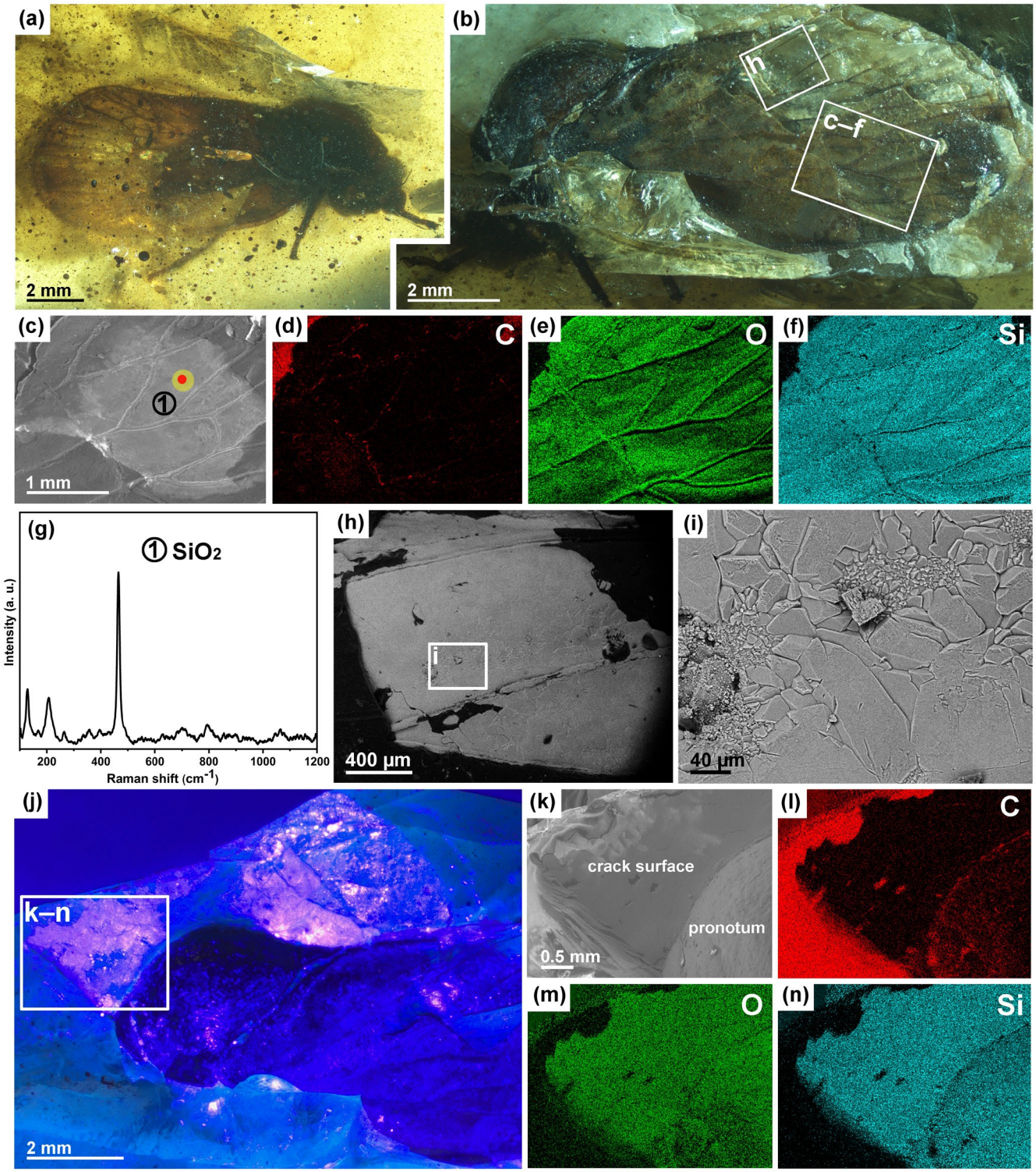

FIGURE 3 Silicified fossils. (a–n) Cicada (Hemiptera: Cicadoidea) (MGM2016–014). a–b, Reflected light micrographs of the right (a) and left (b) lateral views. (c–f) BSE image (b) and EDX elemental maps of (c) for C (d), O (e) and Si (f). (g) Raman spectrum of quartz material located at point in (c). (h) BSE image of box in (b), showing the left hindwing, entirely replaced by quartz. (i) BSE image of box in (h), showing detail of hindwing surface with quartz crystal aggregates. (j) Reflected UV light micrograph of exposed cicada, showing quartz that precipitated in amber cracks and around the insect. (k–n) BSE image and EDX elemental maps of (k) for C (l), O (m) and Si (n) of the cicada pronotum and the connected crack in the amber matrix, showing the quartz that precipitated along cracks within the amber and around the insect

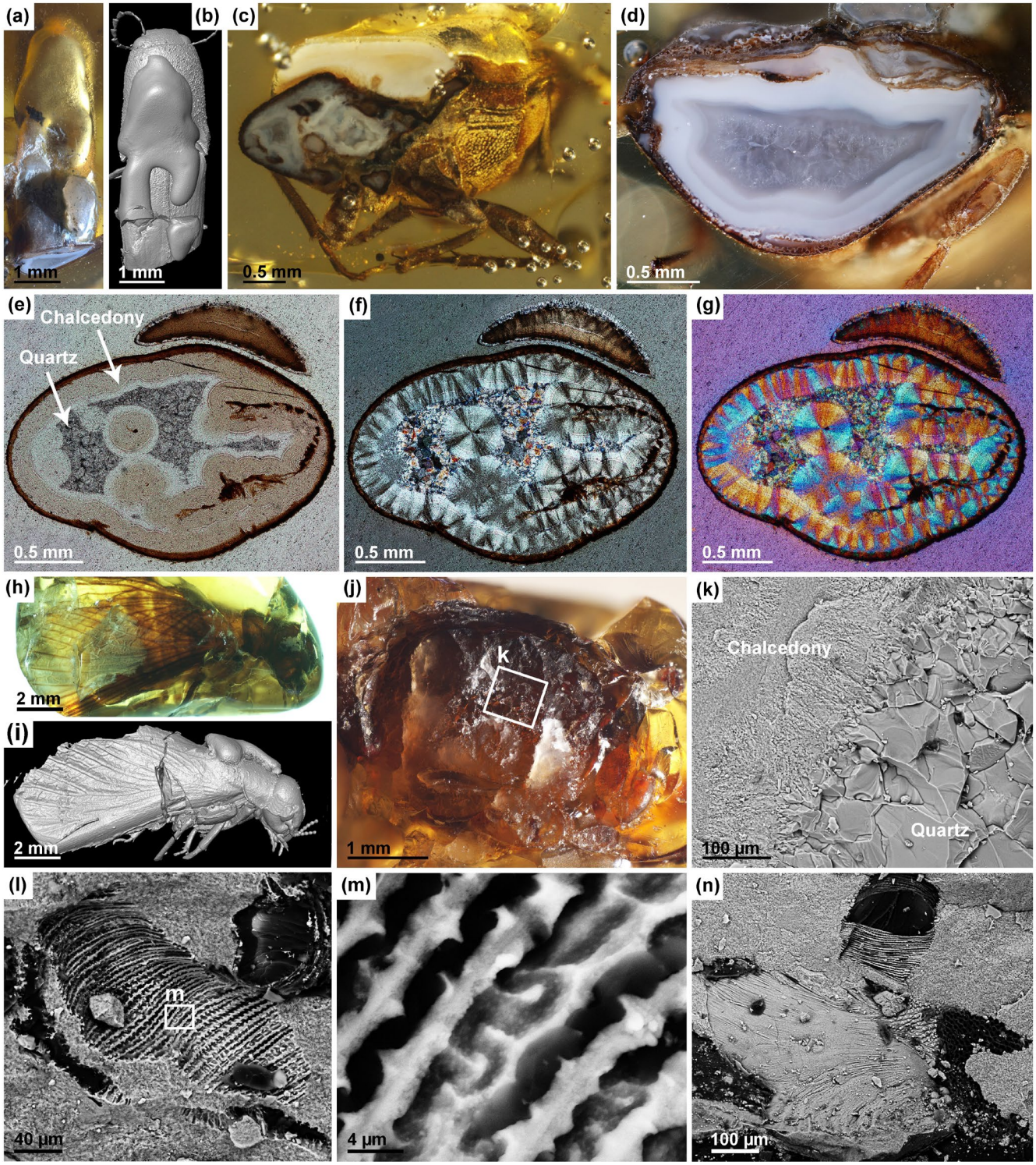

FIGURE 4 Silicified fossils. (a–g) Silicified click beetle (Coleoptera: Elateridae) (MGM2016–015) into agate. (a) Reflected light micrograph of dorsal view. (b) Dorsal view of microtomographic reconstruction. (c–d) Reflected light micrographs of transverse sections. (c) Transverse section of thorax. (d) Transverse section of abdomen. (e–f) Transmitted light micrographs of transverse thin section of thorax (thin section thickness ~60 μm). (e) Brightfield micrograph. (f) Cross polarized light micrograph. (g) Transmitted, cross polarized light micrograph of thorax acquired with a first-order red compensator. (h–n) Drywood termite (Blattodea: Kalotermitidae) (MGM2016–016). (h–i) Right lateral view. (h) Reflected light micrograph. (i) Microtomographic reconstruction. (j) Reflected light micrographs of unpolished transverse section of the abdomen. (k–n) BSE images. (k) Image of box in (j), showing the macro- and microcrystalline quartz. (l–n) Internal structures preserved in microcrystalline quartz of the transverse section. (l) Trachea structure. (m) Magnified image of box in (l), thin and spiral cuticle of tracheae replaced by microcrystalline quartz. (n) Fibre structures and mesh-like structures

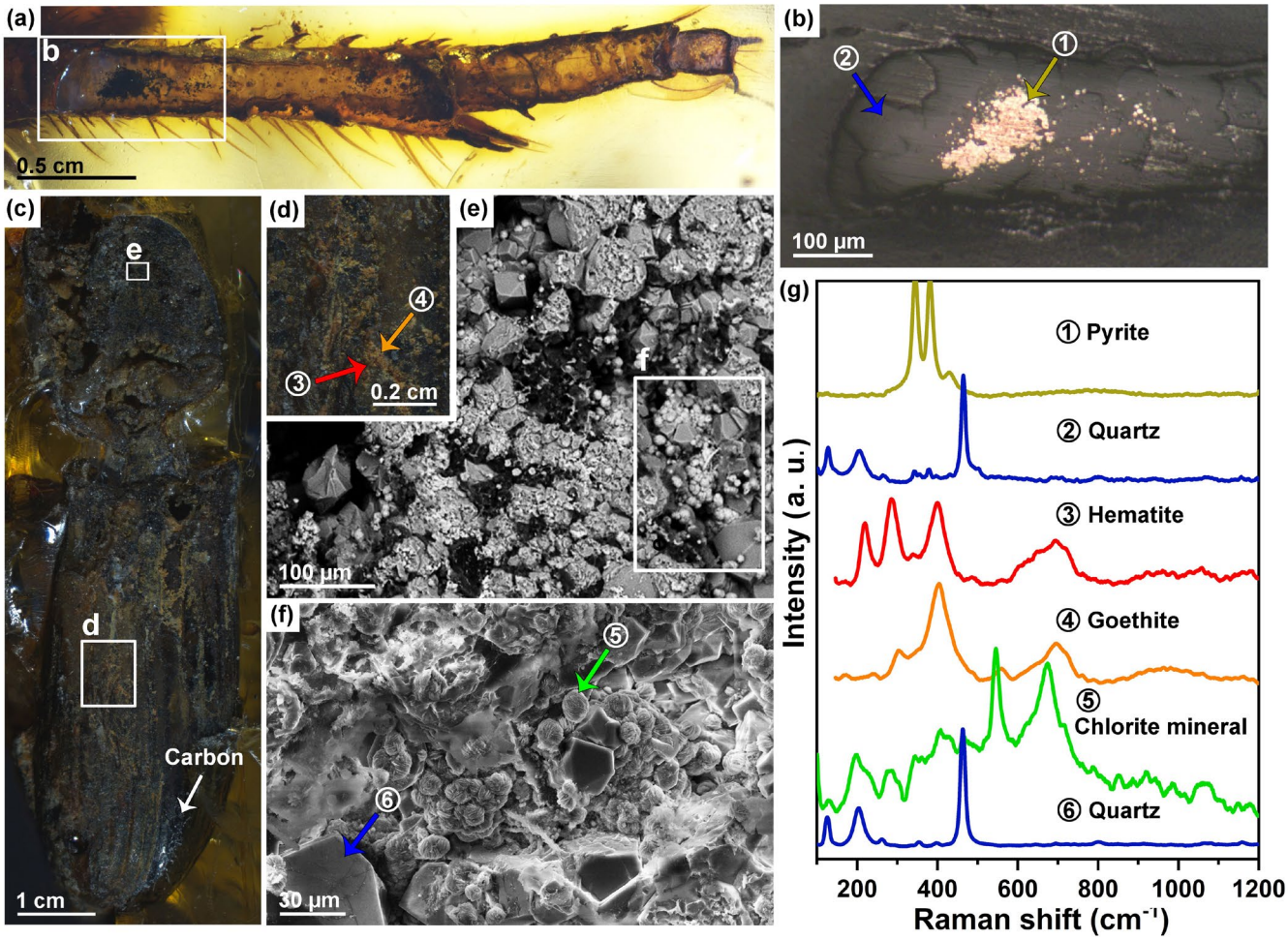

FIGURE 5 Silicified insects with carbonaceous material, pyrite, iron oxide and phyllosilicate minerals. (a–b) Silicified hind leg of cicada nymph (Hemiptera: Cicadoidea) (MGM2016–017) with ferrous iron minerals. (a) Reflected light micrograph. (b) Magnified view of the box in (a) showing pyrite and quartz precipitated in the leg cavity. (c–g) Silicified stag beetle (Coleoptera: Lucanidae) (MGM2016–018) with ferric iron minerals and phyllosilicate minerals. (c) Reflected light micrograph of specimen. (d) Magnified view of the box (c) showing haematite and goethite encrusting the silicified body. (e) BSE image of the box in (c), showing encrustations of haematite and goethite, and carbonaceous material covering euhedral crystals of quartz. (f) Magnified view of the box in (e), showing spherical aggregates of a chlorite group mineral. (g) Raman spectra of carbon, pyrite, quartz, haematite, goethite and chlorite group minerals from the areas indicated by arrows in (b), (c), (d) and (f)

light microscope of the hind leg of a cicada nymph (Hemiptera: Cicadoidea) show that the leg consists of quartz but includes minor amounts of pyrite (Figure 5a,b), which is opaque but highly reflective compared to the surrounding quartz. Likewise, BSE-SEM and Raman spectroscopy show that a stag beetle (Coleoptera: Lucanidae), which mainly consists of euhedral quartz (Figure 5e,f), is encrusted by carbonaceous material and red, brown and yellow minerals (Figure 5c,d), including disordered carbon, haematite, goethite and phyllosilicate minerals that may belong to the chlorite group (Figure 5f,g).

4 | DISCUSSION

To date, there is no record of calcified or silicified insects embedded in amber and both preservational types are rare in the fossil record of insects (Lindgren et al., 2019; Martínez-Delclòs et al., 2004; McCobb et al., 1998; Muscente et al., 2017; Park & Downing, 2001). Here, we provide the first definitive record of calcified and silicified insects embedded in fossil resin. Our results show that the quality and fidelity of morphological preservation depend on the crystallites' sizes in mineralized insects. The two termite specimens in this study notably differ in their quality of preservation, with only one drywood termite retaining small morphological characters (e.g. trachea as well as fibre and mesh-like structures) and the other lacking such fine features. The labile soft tissue structures of the grasshopper and drywood termite specimens are particularly well-preserved, suggesting that calcification and silicification happened rapidly after the biological structures had just started to decay. Nonetheless, even if different insect groups have different body structures with a varying potential to resist degradation and mineralization potential (Parry et al., 2018), the diverse groups of insects in this study suggest that their taphonomic pathways do not depend on taxonomic affinity.

The mineralization of exceptionally preserved fossils depends on the availability of oxidants and reactive chemical species in the microenvironment (water or resin) surrounding the decaying carcass (Briggs, 2003; Briggs & Wilby, 1996a; Mähler et al., 2020; Muscente et al., 2014, 2017; Schiffbauer et al., 2014). Insects generally do not have biomineralized tissues made of silica or calcium carbonate (Li et al., 2020); ergo, the silicification and calcification of the Kachin insects must have been caused by precipitation of chemical species from two sources: (1) decomposition of their tissues in response to microbial respiration and (2) fluid from the surrounding environment (e.g. sediment). Our results give direct evidence that some of the chemical species involved in mineralization (e.g. silicic acid and Ca^{2+}) entered into the amber, inclusions and carcasses through cracks in the resin (e.g. Havelcová et al., 2016; Sadowski et al., 2021). In the cicada specimen, quartz crystals precipitated in the amber cracks along the cicada body (Figure 3j-n). Similarly, in the lacewing larva, the precipitation of calcite filled the lower part of the abdomen along a crack (Figure 2l–m). Such cracks are common in Kachin amber and ambers from other localities. The Kachin amber contains bivalve borings filled with diagenetic minerals (Smith and Ross, 2016). These borings suggest that mineralization occurred after the resin was transported to a calcium-rich marine environment, where it became colonized by piddocks.

A variety of microbial processes likely contributed to the mineralization of the Kachin fossils. The pyrite in the silicified leg of a cicada nymph occurs within quartz, indicating that it formed prior

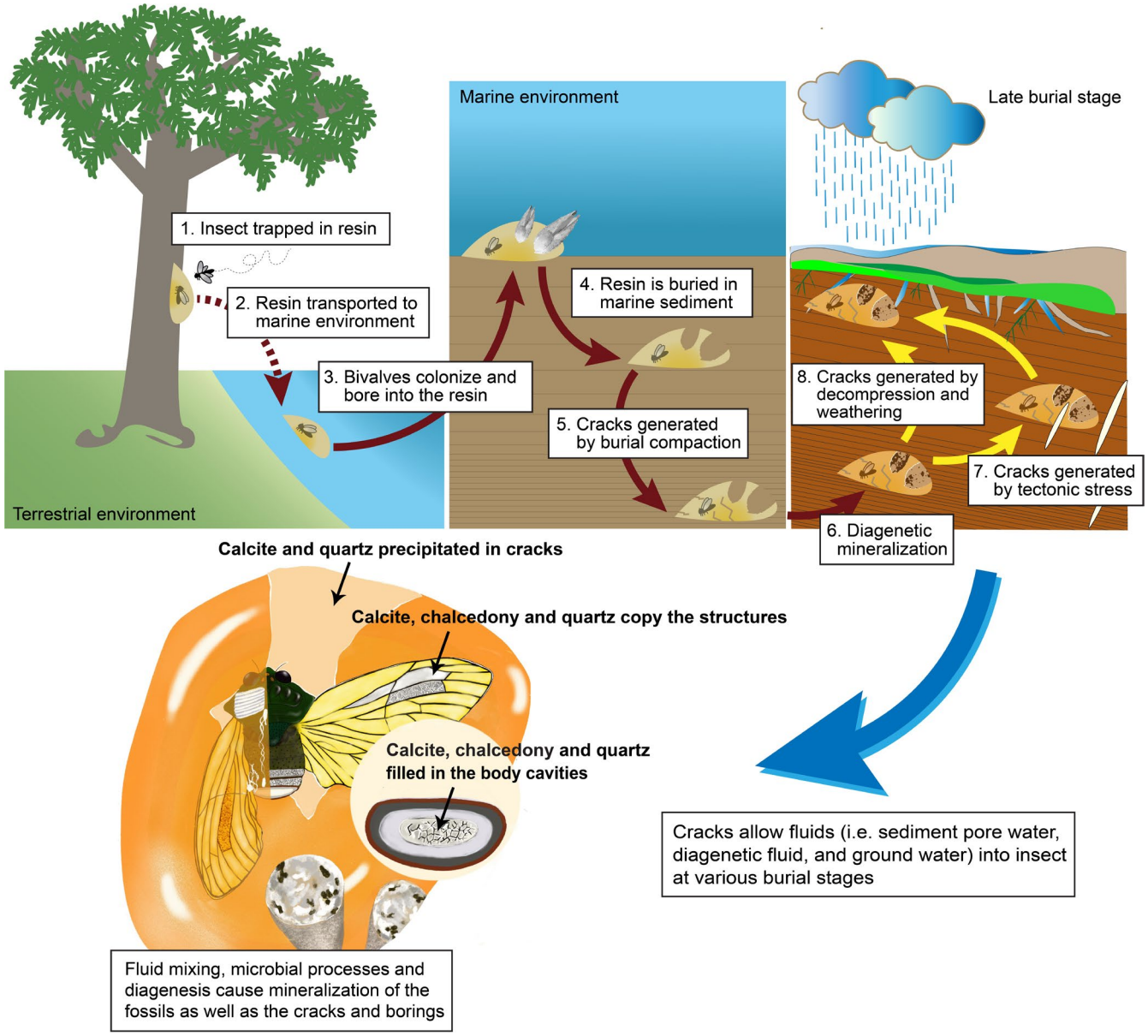

FIGURE 6 Taphonomic model for mineralized insects in Kachin amber. The model implies that the Kachin insect fossils were preserved through successions of events spanning from terrestrial to marine environments. After being buried, the resin (and subsequent amber) was subject to diagenesis, tectonic stress and weathering. Fluids (e.g. sediment pore water, diagenetic fluid and ground water) entered the inclusions at various burial stages throughout its geological history

to silicification. This pyrite represents evidence of microbial sulphate reduction, a form of anaerobic respiration that produces H_2S, which can precipitate as pyrite through reaction with dissolved iron (Muscente et al., 2017; Schiffbauer et al., 2014). In addition to sulphate reduction, other processes like iron reduction and methanogenesis may have also contributed to calcification and silicification. All of these processes generate HCO_3^- that can react with dissolved Ca^{2+} to precipitate as solid calcite (Muscente et al., 2017).

The by-products of microbial respiration (e.g. CO_2) undergo equilibrium reactions, which typically reduce the pH in the microenvironments around decaying carcasses (Xiao et al., 2010). Notably, calcification and silicification are pH-dependent processes, as calcite and silica have opposing solubility–pH relationships over the pH range of approximately 9 to 10 (Knauth, 1994). Consequently, microbial processes that reduce pH can cause a shift from calcite to silica precipitation (Muscente et al., 2014; Xiao et al., 2010). Under the influence of sulphate reduction, acidification of the microenvironments around the Kachin insects likely led to calcite dissolution and silica precipitation. This phenomenon accounts for the grasshopper nymph consisting of both minerals (Figure 1c–g). In this specimen, the calcified structures are better preserved than the silicified features, suggesting that labile tissues were calcified before microbial activity caused a reduction in pore water pH and, thereby, drove the silicification of the remaining substrates.

Silicification occurs in pore water with higher concentrations of dissolved silica than its normal supersaturation level. Source of dissolved silica that may elevate its concentration beyond this supersaturation level includes volcanic vents (Briggs et al., 1996), hydrothermal springs (Konhauser et al., 2001) and clay diagenesis (Muscente et al., 2014). Evaporation of seawater also increases the concentration of silica along coastlines with the limited circulation of water (Maliva et al., 2005). All of these sources may, in part, account for the silicification of fossils. The Kachin amber occurs in close association with volcaniclastic rock (Cruickshank & Ko, 2003) and was preserved in a shallow, nearshore depositional environment (Cruickshank & Ko, 2003), where evaporation of seawater may have influenced dissolved silica levels. The presence of the diagenetic minerals (calcite, quartz and pyrite) suggests that microbial processes may have also played a role by creating low-pH microenvironments, where clay minerals dissolved and released silica to pore water. In any case, silicification caused the concentration of dissolved silica in the microenvironments around the fossils to drop over time. The click beetle and drywood termite specimens contain multiple varieties of quartz, suggesting that the microcrystalline (chalcedonic) quartz precipitated on the substrates of the organisms prior to the formation of macrocrystalline quartz within the body cavities of the specimens (Figure 4d-f,j). This paragenesis indicates that the macrocrystalline quartz precipitated after the chalcedonic quartz as a result of decreasing concentrations of dissolved silica (Heaney, 1993).

The surfaces of some of the silicified fossils (Figure 5c–g) are encrusted by haematite, goethite and phyllosilicate minerals. Given the paragenetic relationships, these minerals must have formed after the pyrite, calcite and quartz. Given that haematite and goethite form in oxidative environments, they most likely originated via the circulation of ferric iron-rich solutions through the cracks in the amber. These solutions may represent diagenetic pore fluids that developed during tectonism or ground water that contributed to terrestrial weathering. In any case, these additional minerals demonstrate that amber is not a closed system—diagenetic solutions and ground water regularly flow through it and alter the preservation of its inclusions. Accordingly, a fossil in amber may undergo multiple phases of diagenetic alteration and experience the effects of chemical weathering.

Given these observations, we hypothesize that the physical and chemical properties of the resin prevented the degradation of the insects until it became buried in marine sediment where a large number of cracks in resin generated during burial compaction phases, thereby exposing the insects to pore water with the reactive chemical species of diagenesis. These chemical species likely fuelled degradation of the insects via microbial processes, which may have created sharp geochemical gradients between the fluids of the inclusions and the fluids outside the amber. Such geochemical gradients can cause the chemical reactions of calcification and silicification (Briggs, 2003; Butts & Briggs, 2011; Muscente et al., 2017; Sagemann et al., 1999). In any case, the cracks allowed for diagenetic fluids to enter the insects, thereby allowing for their mineralization. In the late stage, the Kachin amber may have undergone tectonism, as evidenced by the amber being cut by veins of thin white calcite (Cruickshank & Ko, 2003; Shi et al., 2012), and weathering. Overall, this model implies that the Kachin insect fossils were preserved through successions of events spanning terrestrial and marine environments (Figure 6).

The fossils in this study are not comprised entirely of minerals. A number of specimens contain organic residues (Figures 1a, 2h,i and 3e,f). The organic residues are probably stabilized polymers formed and modified by diagenetic processes (Cody et al., 2011; Georgiou et al., 2019; Stankiewicz et al., 1998, 2000). The presence of organic matter in inclusions may provide opportunities for mineralization. These substrates provide reactive interfaces (e.g. hydrogen bond-forming carbohydrate hydroxyl groups) that may have helped promote nucleation of silica and calcite films that subsequently experienced sustained, autocatalytic and abiogenic growth (Addadi & Weiner, 1985; Konhauser et al., 2001).

In summation, calcification and silicification played important roles in the exceptional preservation of fossils in the Kachin amber. These mineralized fossils, along with cases of pyritized and phosphatized inclusions in Baltic, Spanish, Kachin amber and Dominican amber, indicate that mineralization in amber is more widespread than commonly thought. Resin and amber are not closed microenvironmental systems. Cracks are common in the Kachin amber, as well as in resins, copals and ambers from other localities (e.g. Andersen & Poinar, 1998; Arriaga-Varela et al., 2021; Girard et al.,2009; Grimaldi & Singh, 2012; Poinar, 1992; Schmidt et al., 2018; Seyfullah et al., 2018; Shi et al., 2014, Figure 2b). The cracks had chances to be generated in multiple stages, for instance, amber shrinkage during maturation, fracturing by the overlying sediment and fracturing or augmented by local tectonism (Cruickshank & Ko, 2003). Cracks may

also occur when the resin suffers from heat and smoke by fire, polymerizes in the air, or during transport processes (e.g. Hartl et al., 2015; Seyfullah et al., 2018). The formation of cracks at different stages may cause fluids to contact the amber inclusions at those times and, thereby, affect the paragenesis of minerals in amber. Fluids (e.g. sediment pore water, diagenetic fluid and ground water) at different burial stages can enter amber throughout its geological history, driving the degradation and mineralization of its inclusions. These solutions control the preservational quality and fidelity of amber inclusions and create taphonomic biases that limit the amount of paleobiologic information that can be collected from them.

ACKNOWLEDGMENTS

We thank Thorsten Geisler, Chun-Jung Chen, Renate Radek, Naihua Xue, Peter J. Mill and Hantao Hui for discussions, Suping Wu for help with the micro-computed tomography, Chunzhao Wang for help with SEM operation, and Nils Jung and Olaf Dülfer for help with sample preparation. The authors thank Prof. Butterfield (subject editor) and three anonymous reviewers for comments and suggestions. This research was supported by the Strategic Priority Research Program of the Chinese Academy of Sciences (XDB26000000), the Second Tibetan Plateau Scientific Expedition and Research (2019QZKK0706) and the National Natural Science Foundation of China (42125201, 41688103). F.T., B.M. and M.L. thank the German Research Council (grants GE 1094/24-1396 to Thorsten Geisler, RU 665/12-1 to Jes Rust, within the DFG Research Unit FOR2685) for financial support. This is also contribution number 42 of the DFG Research Unit FOR2685 'The Limits of the Fossil Record'. E.A.J. and J.S. thank the Chinese Academy of Sciences for the support under the President's International Fellowship Initiative (PIFI). This is a Leverhulme Emeritus Fellowship Contribution for E.A.J. Hui Jiang is thankful for the support from the CAS-DAAD Joint Scholarship Program.

CONFLICT OF INTEREST

The authors declare no competing interests.

DATA AVAILABILITY STATEMENT

All data are deposited in the Geobiodiversity Database (GBDB, http://www.geobiodiversity.com) and are available online.

ORCID

Hui Jiang https://orcid.org/0000-0002-7873-5213

REFERENCES

Addadi, L., & Weiner, S. (1985). Interactions between acidic proteins and crystals: stereochemical requirements in biomineralization. *Proceedings of the National Academy of Sciences of the United States of America*, *82*, 4110–4114. https://doi.org/10.1073/pnas.82.12.4110

Andersen, N. M., & Poinar, G. O. (1998). A marine water strider (Hemiptera: Veliidae) from Dominican amber. *Insect Systematics & Evolution*, *29*(1), 1–9. https://doi.org/10.1163/187631298X00131

Arriaga-Varela, E., Brunke, A., Girón, J. C., Szawaryn, K., Bruthansová, J., & Fikáček, M. (2021). Micro-CT reveals hidden morphology and clarifies the phylogenetic position of Baltic amber water scavenger beetles (Coleoptera: Hydrophilidae). *Historical Biology*, *33*(9), 1395–1411. https://doi.org/10.1080/08912963.2019.1699921

Baroni-Urbani, C., & Graeser, S. (1987). REM-Analysen an einer pyritisierten Ameise aus Baltischen Bernstein. *Stuttgarter Beiträge Zur Naturkunde Serie B*, *133*, 1–16.

Barthel, H. J., Fougerouse, D., Geisler, T., & Rust, J. (2020). Fluoridation of a lizard bone embedded in Dominican amber suggests open-system behavior. *PLoS One*, *15*, e0228843. https://doi.org/10.1371/journal.pone.0228843

Briggs, D. E. G. (2003). The role of decay and mineralization in the preservation of soft-bodied fossils. *Annual Review of Earth and Planetary Sciences*, *31*, 275–301. https://doi.org/10.1146/annurev.earth.31.100901.144746

Briggs, D. E. G. (2018). Sampling the insects of the amber forest. *Proceedings of the National Academy of Sciences of the United States of America*, *115*, 6525–6527. https://doi.org/10.1073/pnas.1807017115

Briggs, D. E. G., Siveter, D. J., & Siveter, D. J. (1996). Soft-bodied fossils from a Silurian volcaniclastic deposit. *Nature*, *382*(6588), 248–250. https://doi.org/10.1038/382248a0

Briggs, D. E. G., & Wilby, P. R. (1996). The role of the calcium carbonate-calcium phosphate switch in the mineralization of soft-bodied fossils. *Journal of the Geological Society*, *153*, 665–668. https://doi.org/10.1144/gsjgs.153.5.0665

Butts, S. H., & Briggs, D. E. G. (2011). Silicification through time. In P. A. Allison, & D. J. Bottjer (Eds.), *Taphonomy: Process and bias through time* (pp. 411–434). Springer.

Cody, G. D., Gupta, N. S., Briggs, D. E. G., Kilcoyne, A. L. D., Summons, R. E., Kenig, F., Plotnick, R. E., & Scott, A. C. (2011). Molecular signature of chitin-protein complex in Paleozoic arthropods. *Geology*, *39*, 255–258. https://doi.org/10.1130/G31648.1

Cruickshank, R. D., & Ko, K. O. (2003). Geology of an amber locality in the Hukawng Valley, Northern Myanmar. *Journal of Asian Earth Sciences*, *21*(5), 441–455. https://doi.org/10.1016/S1367-9120(02)00044-5

Georgiou, R., Gueriau, P., Sahle, C. J., Bernard, S., Mirone, A., Garrouste, R., Bergmann, U., Rueff, J.-P., & Bertrand, L. (2019). Carbon speciation in organic fossils using 2D to 3D x-ray Raman multispectral imaging. *Science Advances*, *5*(8), eaaw5019. https://doi.org/10.1126/sciadv.aaw5019

Girard, V., Neraudeau, D., Breton, G., Martin, S. S., & Martin, J.-P.-S. (2009). Contamination of amber samples by recent microorganisms and remediation evidenced by Mid-Cretaceous amber of France. *Geomicrobiology Journal*, *26*(1), 21–30. https://doi.org/10.1080/01490450802599268

Grimaldi, D. A., Bonwich, E., Delannoy, M., & Doberstein, S. (1994). Electron microscopic studies of mummified tissues in amber fossils. *American Museum Novitates*, *3097*, 1–31.

Grimaldi, D. A., Engel, M. S., & Nascimbene, P. C. (2002). Fossiliferous Cretaceous amber from Myanmar (Burma): Its rediscovery, biotic diversity, and paleontological significance. *American Museum Novitates*, *2002*, 1–71. https://doi.org/10.1206/0003-0082(2002)361<0001:FCAFMB>2.0.CO;2

Grimaldi, D., & Singh, H. (2012). The extinct genus Pareuthychaeta in Eocene ambers (Diptera: Schizophora: ephydroidea). *The Canadian Entomologist*, *144*(1), 17–28. https://doi.org/10.4039/tce.2012.5

Hartl, C., Schmidt, A. R., Heinrichs, J., Seyfullah, L. J., Schäfer, N., Gröhn, C., Rikkinen, J., & Kaasalainen, U. (2015). Lichen preservation in amber: morphology, ultrastructure, chemofossils, and taphonomic alteration. *Fossil Record*, *18*(2), 127–135. https://doi.org/10.5194/fr-18-127-2015

Havelcová, M., Machovič, V., Mizera, J., Sýkorová, I., René, M., Borecká, L., Lapčák, L., Bičáková, O., Janeček, O., & Dvořák, Z. (2016). Structural changes in amber due to uranium mineralization. *Journal of Environmental Radioactivity*, *158–159*, 89–101. https://doi.org/10.1016/j.jenvrad.2016.04.004

Heaney, P. J. (1993). A proposed mechanism for the growth of chalcedony. *Contributions to Mineralogy and Petrology*, *115*, 66–74. https://doi.org/10.1007/BF00712979

Henwood, A. (1992a). Exceptional preservation of dipteran flight muscle and the taphonomy of insects in amber. *Palaios*, *7*, 203–212. https://doi.org/10.2307/3514931

Henwood, A. A. (1992b). Soft-part preservation of beetles in Tertiary amber from the Dominican Republic. *Palaeontology*, *35*(4), 901–912. https://doi.org/10.1098/rspb.2004.2939

Knauth, L. P. (1994). Petrogenesis of chert. In P. J. Heaney, C. T. Prewitt & G. V. Gibbs (Eds.), *Silica: Physical behavior, geochemistry and materials applications*. Reviews in Mineralogy and Geochemistry (Vol. *29*, pp. 233–258). De Gruyter. https://doi.org/10.1515/9781501509698-012

Koller, B., Schmitt, J. M., & Tischendorf, G. (2005). Cellular fine structures and histochemical reactions in the tissue of a cypress twig preserved in Baltic amber. *Proceedings of the Royal Society B: Biological Sciences*, *272*(1559), 121–126.

Konhauser, K. O., Phoenix, V. R., Bottrell, S. H., Adams, D. G., & Head, I. M. (2001). Microbial–silica interactions in Icelandic hot spring sinter: possible analogues for some Precambrian siliceous stromatolites. *Sedimentology*, *48*, 415–433. https://doi.org/10.1046/j.1365-3091.2001.00372.x

Kowalewska, S., & Szwedo, J. (2009). Examination of the Baltic amber inclusion surface using SEM techniques and X-ray microanalysis. *Palaeogeography, Palaeoclimatology, Palaeoecology*, *271*, 287–291. https://doi.org/10.1016/j.palaeo.2008.10.025

Laflamme, M., Schiffbauer, J. D., & Darroch, S. A. F. (2014). Amber. In M. Laflamme, J. D. Schiffbauer, & S. A. F. Darroch (Eds.), *Reading and writing of the fossil record. Preservational pathways to exceptional fossilization*, *20* (pp. 164–216). The Paleontological Society Papers. https://doi.org/10.1017/S108933260000276X

Langenheim, J. H. (2003). *Plant resins: Chemistry, evolution, ecology, and ethnobotany*. Timber Press.

Li, H., Sun, C. -Y., Fang, Y., Carlson, C. M., Xu, H., Ješovnik, A., Sosa-Calvo, J., Zarnowski, R., Bechtel, H. A., Fournelle, J. H., Andes, D. R., Schultz, T. R., Gilbert, P. U. P. A., & Currie, C. R. (2020). Biomineral armor in leaf-cutter ants. *Nature Communications*, *11*(1), 5792. https://doi.org/10.1038/s41467-020-19566-3

Lindgren, J., Nilsson, D.-E., Sjövall, P., Jarenmark, M., Ito, S., Wakamatsu, K., Kear, B. P., Schultz, B. P., Sylvestersen, R. L., Madsen, H., LaFountain, J. R. Jr, Alwmark, C., Eriksson, M. E., Hall, S. A., Lindgren, P., Rodríguez-Meizoso, I., & Ahlberg, P. (2019). Fossil insect eyes shed light on trilobite optics and the arthropod pigment screen. *Nature*, *573*, 122–125. https://doi.org/10.1038/s41586-019-1473-z

Lozano, R. P., Pérez-de la Fuente, R., Barrón, E., Rodrigo, A., Viejo, J. L., & Peñalver, E. (2020). Phloem sap in Cretaceous ambers as abundant double emulsions preserving organic and inorganic residues. *Scientific Reports*, *10*(1), 1–15. https://doi.org/10.1038/s41598-020-66631-4

Mähler, B., Janssen, K., Menneken, M., Tahoun, M., Lagos, M., Bierbaum, G., Müller, C. E., & Rust, J. (2020). Calcite precipitation forms crystal clusters and muscle mineralization during the decomposition of *Cambarellus diminutus* (Decapoda: Cambaridae) in freshwater. *Palaeontologia Electronica*, *23*, a55. https://doi.org/10.26879/992

Maliva, R. G., Knoll, A. H., & Simonson, B. M. (2005). Secular change in the Precambrian silica cycle: Insights from chert petrology. *Geological Society of America Bulletin*, *117*, 835–845. https://doi.org/10.1130/B25555.1

Martínez-Delclòs, X., Briggs, D. E. G., & Peñalver, E. (2004). Taphonomy of insects in carbonates and amber. *Palaeogeography, Palaeoclimatology, Palaeoecology*, *203*, 19–64. https://doi.org/10.1016/S0031-0182(03)00643-6

Martín-González, A., Wierzchos, J., Gutiérrez, J.-C., Alonso, J., & Ascaso, C. (2009). Double fossilization in eukaryotic microorganisms from Lower Cretaceous amber. *BMC Biology*, *7*, 9. https://doi.org/10.1186/1741-7007-7-9

McCobb, L. M. E., Duncan, I. J., Jarzembowski, E. A., Stankiewicz, B. A., Wills, M. A., & Briggs, D. E. G. (1998). Taphonomy of the insects from the insect bed (Bembridge Marls), late Eocene, Isle of Wight, England. *Geological Magazine*, *135*, 553–563. https://doi.org/10.1017/S0016756898001204

McCoy, V. E., Soriano, C., & Gabbott, S. E. (2018). A review of preservational variation of fossil inclusions in amber of different chemical groups. *Earth and Environmental Science Transactions of the Royal Society of Edinburgh*, *42*, 119–136. https://doi.org/10.1017/S1755691017000391

McCoy, V. E., Soriano, C., Pegoraro, M., Luo, T., Boom, A., Foxman, B., & Gabbott, S. E. (2018). Unlocking preservation bias in the amber insect fossil record through experimental decay. *PLoS One*, *13*, e0195482. https://doi.org/10.1371/journal.pone.0195482

Muscente, A. D., Hawkins, A. D., & Xiao, S. (2014). Fossil preservation through phosphatization and silicification in the Ediacaran Doushantuo Formation (South China): a comparative synthesis. *Palaeogeography, Palaeoclimatology, Palaeoecology*, *434*, 46–62. https://doi.org/10.1016/j.palaeo.2014.10.013

Muscente, A. D., Schiffbauer, J. D., Broce, J., Laflamme, M., O'Donnell, K., Boag, T. H., Meyer, M., Hawkins, A. D., Huntley, J. W., McNamara, M., MacKenzie, L. A., Stanley, G. D. Jr, Hinman, N. W., Hofmann, M. H., & Xiao, S. (2017). Exceptionally preserved fossil assemblages through geologic time and space. *Gondwana Research*, *48*, 164–188. https://doi.org/10.1016/j.gr.2017.04.020

Muscente, A. D., & Xiao, S. (2015). Resolving three-dimensional and subsurficial features of carbonaceous compressions and shelly fossils using backscattered electron scanning electron microscopy (BSE-SEM). *Palaios*, *30*, 462–548. https://doi.org/10.2110/palo.2014.094

Park, L. E., & Downing, K. F. (2001). Paleoecology of an exceptionally preserved arthropod fauna from lake deposits of the Miocene Barstow Formation, Southern California, USA. *Palaios*, *16*, 175–184. https://doi.org/10.1669/0883-1351(2001)016<0175:POAEPA>2.0.CO;2

Parry, L. A., Smithwick, F., Nordén, K. K., Saitta, E. T., Lozano-Fernandez, J., Tanner, A. R., Caron, J.-B., Edgecombe, G. D., Briggs, D. E. G., & Vinther, J. (2018). Soft-bodied fossils are not simply rotten carcasses - toward a holistic understanding of exceptional fossil preservation. *BioEssays*, *40*(1), 1700167. https://doi.org/10.1002/bies.201700167

Penney, D. (2010). *Biodiversity of fossils in Amber from the major world deposits*. Siri Scientific Press.

Poinar, G. O. Jr (1992). *Life in Amber*. Stanford University Press.

Poinar, G. O. Jr, & Hess, R. (1982). Ultrastructure of 40-million-year-old insect tissue. *Science*, *215*, 1241–1242. https://doi.org/10.1126/science.215.4537.1241

Ross, A. J. (2021). Supplement to the Burmese (Myanmar) amber checklist and bibliography, 2020. *Palaeoentomology*, *4*(1), 57–76. https://doi.org/10.11646/PALAEOENTOMOLOGY.4.1.11

Rust, J., Singh, H., Rana, R. S., McCann, T., Singh, L., Anderson, K., Sarkar, N., Nascimbene, P. C., Stebner, F., Thomas, J. C., Solorzano Kraemer, M., Williams, C. J., Engel, M. S., Sahni, A., & Grimaldi, D. (2010). Biogeographic and evolutionary implications of a diverse paleobiota in amber from the early Eocene of India. *Proceedings of the National Academy of Sciences of the United States of America*, *107*(43), 18360–18365. https://doi.org/10.1073/pnas.1007407107

Sadowski, E. M., Schmidt, A. R., Seyfullah, L. J., & Kunzmann, L. (2017). Conifers of the" Baltic Amber Forest" and their palaeoecological significance. *Stapfia*, *106*, 1–73.

Sadowski, E.-M., Schmidt, A. R., Seyfullah, L. J., Solórzano-Kraemer, M. M., Neumann, C., Perrichot, V., Hamann, C., Milke, R., & Nascimbene, P. C. (2021). Conservation, preparation and imaging of diverse ambers and their inclusions. *Earth-Science Reviews*, *220*, 103653. https://doi.org/10.1016/j.earscirev.2021.103653

Sagemann, J., Bale, S. J., Briggs, D. E. G., & Parkes, R. J. (1999). Controls on the formation of authigenic minerals in association with decaying organic matter: an experimental approach. *Geochimica Et Cosmochimica Acta*, *63*, 1083–1095. https://doi.org/10.1016/S0016-7037(99)00087-3

Schiffbauer, J. D., Xiao, S., Cai, Y., Wallace, A. F., Hua, H., Hunter, J., Xu, H., Peng, Y., & Kaufman, A. J. (2014). A unifying model for Neoproterozoic-Palaeozoic exceptional fossil preservation through pyritization and carbonaceous compression. *Nature Communications*, *5*, 5754. https://doi.org/10.1038/ncomms6754

Schmidt, A. R., Kaulfuss, U., Bannister, J. M., Baranov, V., Beimforde, C., Bleile, N., Borkent, A., Busch, A., Conran, J. G., Engel, M. S., Harvey, M., Kennedy, E. M., Kerr, P. H., Kettunen, E., Kiecksee, A. P., Lengeling, F., Lindqvist, J. K., Maraun, M., Mildenhall, D. C., … Lee, D. E. (2018). Amber inclusions from New Zealand. *Gondwana Research*, *56*, 135–146. https://doi.org/10.1016/j.gr.2017.12.003

Seyfullah, L. J., Beimforede, C., Corso, J. D., Perrichot, V., Rikkinen, J., & Schmidt, A. R. (2018). Production and preservation of resins–past and present. *Biological Reviews*, *93*, 1684–1714. https://doi.org/10.1111/brv.12414

Seyfullah, L. J., & Schmidt, A. R. (2015). Fossil focus: Stuck in time–life trapped in amber. *Palaeontology*, *5*(12), 1–11.

Shi, G., Dutta, S., Paul, S., Wang, B., & Jacques, F. M. (2014). Terpenoid compositions and botanical origins of Late Cretaceous and Miocene amber from China. *PLoS One*, *9*(10), e111303. https://doi.org/10.1371/journal.pone.0111303

Shi, G., Grimaldi, D. A., Harlow, G. E., Wang, J., Wang, J., Yang, M., Lei, W., Li, Q., & Li, X. (2012). Age constraint on Burmese amber based on U-Pb dating of zircons. *Cretaceous Research*, *37*, 155–163. https://doi.org/10.1016/j.cretres.2012.03.014

Smith, R. D. A., & Ross, A. J. (2016). Amberground pholadid bivalve borings and inclusions in Burmese amber: implications for proximity of resin-producing forests to brackish waters, and the age of the amber. *Earth and Environmental Science Transactions of the Royal Society of Edinburgh*, *107*(2-3), 239–247. https://doi.org/10.1017/S1755691017000287

Stankiewicz, B. A., Briggs, D. E. G., Michels, R., Collinson, M. E., Flannery, M. B., & Evershed, R. P. (2000). Alternative origin of aliphatic polymer in kerogen. *Geology*, *28*, 559–562. https://doi.org/10.1130/0091-7613(2000)28<559:AOOAPI>2.0.CO;2

Stankiewicz, B. A., Poinar, H. N., Briggs, D. E. G., Evershed, R. P., & Poinar, G. O. Jr (1998). Chemical preservation of plants and insects in natural resins. *Proceedings of the Royal Society of London. Series B: Biological Sciences*, *265*, 641–647. https://doi.org/10.1098/rspb.1998.0342

Xiao, S., Schiffbauer, J. D., McFadden, K. A., & Hunter, J. (2010). Petrographic and SIMS pyrite sulfur isotope analyses of Ediacaran chert nodules: Implications for microbial processes in pyrite rim formation, silicification, and exceptional fossil preservation. *Earth and Planetary Science Letters*, *97*, 481–495. https://doi.org/10.1016/j.epsl.2010.07.001

Yu, T., Kelly, R., Mu, L., Ross, A., Kennedy, J., Broly, P., Xia, F., Zhang, H., Wang, B., & Dilcher, D. (2019). An ammonite trapped in Burmese amber. *Proceedings of the National Academy of Sciences of the United States of America*, *116*, 11345–11350. https://doi.org/10.1073/pnas.1821292116

SUPPORTING INFORMATION

Additional supporting information may be found in the online version of the article at the publisher's website.

How to cite this article: Jiang, H., Tomaschek, F., Muscente, A. D., Niu, C., Nyunt, T. T., Fang, Y., Schmidt, U., Chen, J., Lönartz, M., Mähler, B., Wappler, T., Jarzembowski, E. A., Szwedo, J., Zhang, H., Rust, J., & Wang, B. (2022). Widespread mineralization of soft-bodied insects in Cretaceous amber. *Geobiology*, 20, 363–376. https://doi.org/10.1111/gbi.12488